



Acoustic Characterization of a Hybrid Liner Consisting of Porous Material by Using A Unified Linearized Navier-Stokes Approach

W. Na* and S. Boij †

KTH Aeronautical and Vehicle Engineering, Stockholm, Sweden

G. Efraimsson ‡

KTH Aeronautical and Vehicle Engineering, Centre for ECO2 Vehicle Design, Stockholm, Sweden

In this paper, the acoustic properties of a hybrid liner placed at the end of an impedance tube are investigated using numerical simulations. The hybrid liner constitutes of three components, a perforated plate, a porous layer and a rectangular back cavity. The presence of the porous layer is to enhance the absorptive performance of a liner. The main objective of the paper is to verify the proposed numerical methodology - a unified linearized Navier-Stokes Equations (LNSE) approach. In the unified LNSE approach, the combination of the Helmholtz Equation, LNSE as well as the equivalent fluid model are solved in different regions of the impedance tube. To achieve this, the continuity of the coupling condition between the LNSE and the Helmholtz equation is examined. Another objective is to analyze the effectiveness of the porous material to the acoustic performance of the liner. Acoustic liner simulations with and without porous material, porous material with different flow resistivity are carried out. A good agreement is found between the numerical results and the measurements previously performed at KTH MWL.¹

Compared to previous work^{2,3,4}, several improvements have been made in the numerical methodology, such as that the energy equation has been added in order to include the damping due to viscous dissipation as well as the thermal dissipation in the vicinity of the perforated plate.

I. Introduction

Fan noise in aero-engines can be effectively reduced through the installation of acoustic liners as wall treatments in the inlet ducts. Due to the increasing demand of the noise reduction, development of liners giving more absorption and working in a wider frequency range is an active area of research. Usually, single-degree-of-freedom liners (SDOF) are sandwich panels with a basic configuration, consisting of a face-sheet bonded to a honeycomb layer and closed by a back-skin. In this paper, the face-sheet is made by both a perforated plate and a porous metallic foam. This type of the face-sheet made of the absorbing material is expected to enhance the acoustic absorption of the liner. In the paper, a numerical methodology - the Unified LNSE Approach is presented and the effectiveness of the porous material to the acoustic performance of the liner is investigated numerically. Furthermore, the numerical results are compared with the measurements performed at KTH MWL by Kabra et al.¹

In the simulations presented in this paper, different regions of the impedance tube are modeled using different equations. This is done in order to have as fast simulations as possible without sacrificing the accuracy of the results. The linearized Navier-Stokes equations in frequency domain (LNSE) is applied in the vicinity of the perforated plate, while an equivalent fluid model is used in the porous metallic foam. The Helmholtz equation is solved in the main duct and in the back cavity, see Fig. 1, where viscous effects are

*PhD Candidate

†Associate professor and AIAA Member.

‡Professor and AIAA Member.

assumed to be negligible. The LNSE and the equivalent fluid model used in this paper are described in Secs A–B. With different equations applied in different regions of the computational domain, coupling conditions become necessary at the interfaces between the different equations. These coupling conditions are presented in subsection C.

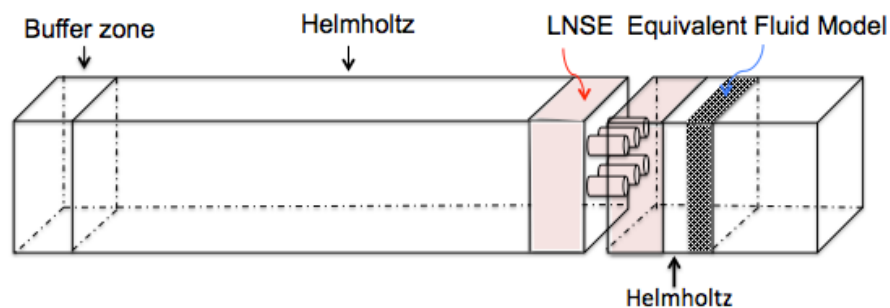


Figure 1. Schematic sketch of the numerical model of the impedance tube

In the experiments, the perforated plate is placed on the top of the cavities, while the metallic foam is compressed into the perforated plate. In the numerical simulations, the perforated plate and the metallic foam are two different layers. The differences of the liner between the numerical modelling and the experimental test samples are illustrated in the Fig. 2. and a photo of the experimental test samples is provided as well as Fig. 3.

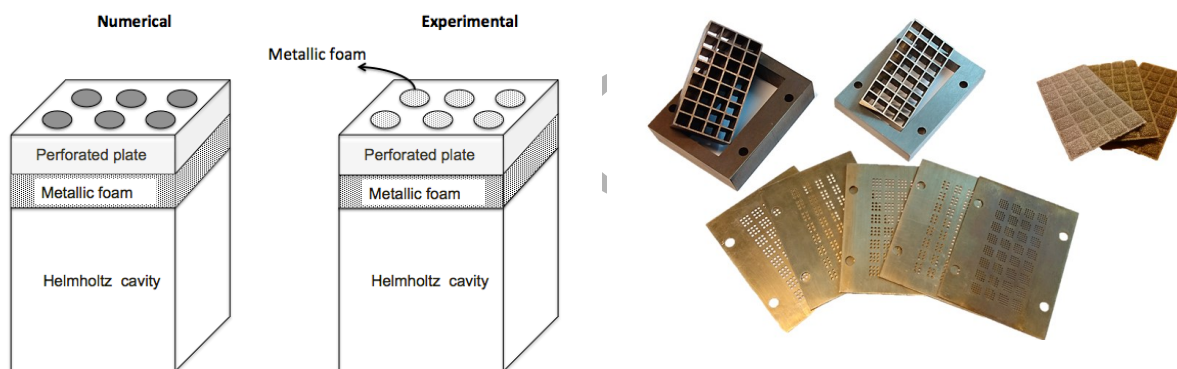


Figure 2. The differences illustrated between the numerical modelling and the experimental test samples.

Figure 3. Experimental test samples of the components of the liner, left upper are the cavities, right upper are the porous metallic foams, and lower are the perforated plates.

II. Numerical Methodology - A Unified LNSE approach

In this section, we first present the three-dimensional Linearized Navier-Stokes equations (LNSE) in frequency domain where the energy equation is also considered. Thereafter the “Unified LNSE approach” which combines the LNSE with the equivalent fluid model and the Helmholtz equation, respectively, are introduced. The proposed “Unified LNSE approach” is capable to model the sound attenuation in the perforated plate, the sound propagation in the porous material and the tube and back cavity in a very efficient way. We also present coupling conditions between the LNSE and Helmholtz equation. By achieving the coupling between the LNSE and the Helmholtz equation, the LNSE can be switched to a Helmholtz equation to reduce the computational cost in the regions where damping or absorbing effects can be considered as negligible. For example, in the hybrid liner, the Helmholtz equation is solved in the main duct, in which only plane waves are propagating without any losses. In this way, around one million degrees of freedom

(DOF) out of 2 million in total are saved in the simulations.

A. Linearized Navier-Stokes equations in frequency domain

The full compressible Navier-Stokes equations in tensor form in a Cartesian coordinate system, with the assumptions of ideal gas and constant specific heat capacity are:⁵

$$\frac{D\rho}{Dt} + \rho \frac{\partial u_i}{\partial x_i} = 0 \quad (1)$$

$$\rho \frac{Du_i}{Dt} = -\frac{\partial p}{\partial x_i} + \mu_B \frac{\partial^2 u_j}{\partial x_i \partial x_j} + \frac{\partial \tau_{ij}}{\partial x_j} + \rho F_i \quad (2)$$

where ρ is the density, p is the pressure, u_i is the i component of the velocity in the Cartesian coordinates, μ_B is the bulk viscosity, which is used to take into account the rotational and translational modes of molecular motion from mutual thermodynamics equilibrium.⁶ F_i is the body force, τ_{ij} is the shear strain rate tensor defined as

$$\tau_{ij} = \mu \left(\frac{\partial u_i}{\partial x_j} + \frac{\partial u_j}{\partial x_i} - \frac{2}{3} \frac{\partial u_k}{\partial x_k} \delta_{ij} \right) \quad (3)$$

where δ_{ij} the Kronecker delta function, μ is the dynamic viscosity.

The energy equation for the fluid with constant specific heat capacity is

$$\frac{\partial T}{\partial t} + u_j \frac{\partial T}{\partial x_j} = \frac{1}{c_p \rho} \left(\frac{\partial p}{\partial t} + u_j \frac{\partial p}{\partial x_j} \right) + \frac{\phi}{c_p \rho} + \frac{1}{c_p \rho} \frac{\partial}{\partial x_j} \left(\kappa_{th} \frac{\partial T}{\partial x_j} \right) \quad (4)$$

where T is the temperature, c_p is the heat capacity at constant pressure, κ_{th} is the thermal conductivity and ϕ is the dissipation of mechanical energy due to the shear viscosity and the fluid relaxation losses, which is defined as:

$$\phi = \mu \left[\frac{\partial u_i}{\partial x_j} \frac{\partial u_i}{\partial x_j} + \frac{\partial u_j}{\partial x_i} \frac{\partial u_i}{\partial x_j} - \left(\frac{2}{3} - \frac{\mu_B}{\mu} \right) \left(\frac{\partial u_i}{\partial x_i} \right)^2 \right] \quad (5)$$

The energy equation is included to replace the isentropic relation previously used by Kierkegaard et al.² The presence of the energy equation gives the possibility to include the effects of heat conduction as well as energy losses in the acoustic boundary layer. The temperature perturbations in the vicinity of the small holes within the perforated plate imply a small modification of the properties of the medium, which has never been taken into account in previous studies^{2,4}

In order to obtain the linearised Navier-Stokes equations in frequency domain, we linearize Eqs (1), (2) and (4), around a steady state solution in time, but varying in space. Thereafter, the perturbed quantities are assumed to have a harmonic time-dependence. Hence, any perturbed quantity q' can be represented as $q'(x, \omega, t) = Re\{\hat{q}(x)e^{-i\omega t}\}$, where \hat{q} is a complex quantity and ω is the angular frequency. By setting $\mathbf{u}_0 = 0$ and $\rho_0 = const$, the linearized continuity equation, linearized momentum equation and linearized energy equation at quiescent medium arrive at⁷

$$-i\omega \hat{\rho} + \rho_0 \nabla \cdot \hat{\mathbf{u}} = 0 \quad (6)$$

$$-i\omega \rho_0 \hat{\mathbf{u}} = -\nabla \cdot \left[P\mathbf{I} + \mu(\nabla \hat{\mathbf{u}} + (\nabla \hat{\mathbf{u}})^T) - \left(\frac{2}{3}\mu - \mu_B \right) (\nabla \cdot \hat{\mathbf{u}}) \right] \quad (7)$$

$$-i\omega(\rho_0 C_p T - T_0 \alpha_0 p) = -\nabla \cdot (-\kappa \nabla T) + Q \quad (8)$$

where a hat $\hat{\cdot}$ indicates a perturbed quantity, a subscript zero indicates mean flow quantities, ρ is the density, \mathbf{u} is the velocity vector, \mathbf{F} is a volume force, ω is the angular frequency and μ is the dynamic viscosity, κ is the thermal conductivity, α_0 is the coefficient of thermal expansion (isobaric), and Q is a possible heat source;

Finally, the linearized equation of state relates the variations in pressure, temperature, and density

$$\rho = \rho_0(\beta_T p - \alpha_0 T) \quad (9)$$

where β_T is the isothermal compressibility.

B. An equivalent fluid model

An equivalent fluid model is a common way to model sound propagation in porous materials. In an equivalent fluid model the sound is assumed to propagate homogeneously in the medium under the exposure of a medium specific damping. The sound propagation in the porous material is then described as a propagation in the “fluid” with the damping properties.

An equivalent fluid model originates from a simple Helmholtz type equation. The effective change compared to a pure Helmholtz equation is that the wave number is altered to take damping, such as viscous losses, into account, i.e.

$$(\nabla^2 + k_{eq}^2)\hat{p} = 0 \quad (10)$$

where k_{eq} is the altered wavenumber that replaces the ordinary wavenumber $k = \omega/c$. The Delany-Bazley model⁸ is the most common equivalent fluid model, and is well validated and used in many industrial applications. Here, the modified wavenumber relates to the original wavenumber as:

$$k_{eq} = \frac{\omega}{c_0} (1 + 0.0978X^{-0.700} - i0.189X^{-0.595}) \quad (11)$$

where

$$X = \frac{\rho_0 f}{\sigma} \quad (12)$$

and the constants such as 0.0978, -0.700 and 0.189 are found from curve fitting of the experimental data. The validity of the model is $10^{-2} < f/\sigma < -1$. If the porosity ϕ is taken into account, we have:

$$X \rightarrow X' = \frac{\rho_0 f}{\sigma \phi} \quad (13)$$

where ρ_0 and c_0 are the density and speed of sound in the air as if no porous material, respectively, and σ is the flow resistivity of the porous material. The unit of the flow resistivity is $[\sigma] = 1Nm^{-4}s$, and typical values are within the range $10^3 < \sigma < 10^5$.

C. Coupling conditions

The LNSE (6)(7)(8) are written in terms of the density perturbation $\hat{\rho}$, while the equivalent fluid model-Helmholtz type equation is expressed in terms of pressure perturbation \hat{p} . From the momentum equation, we have:

$$-i\omega\hat{\rho} + \rho_0\nabla \cdot \hat{\mathbf{u}} = 0 \quad (14)$$

By inserting Eq (14) into the left hand side of Eq. (7) and applying the Gauss theorem, the coupling condition for the momentum equation is obtained as well, namely

$$-\mathbf{n} \cdot \left[PI + \mu(\nabla\hat{\mathbf{u}} + (\nabla\mathbf{u})^T) - \left(\frac{2}{3}\mu - \mu_B\right)(\nabla \cdot \hat{\mathbf{u}}) \right] = P \cdot \mathbf{n} \quad (15)$$

Finally, the coupling condition for the energy equation is obtained by assuming that there is no heat flow into or out of the interfaces, in another words, the flow is adiabatic.

$$-\mathbf{n} \cdot (-\kappa\nabla T) = 0 \quad (16)$$

By applying a coupling condition on the interface as the Eqs. (14)(15)(16), the density perturbation $\hat{\rho}$ is eliminated from the equation, meanwhile, the pressure and velocity perturbations can be ensured continuous.

III. Numerical setup

The computational domain used in the simulations are presented in Fig. 1. Plane waves are prescribed at the upstream end of the impedance tube, where the sound excitation is from $1500Hz$ to $5500Hz$ yielding that the maximum wavelength of the acoustic wave is $226.7mm$ and the minimum wavelength is $7.2mm$.

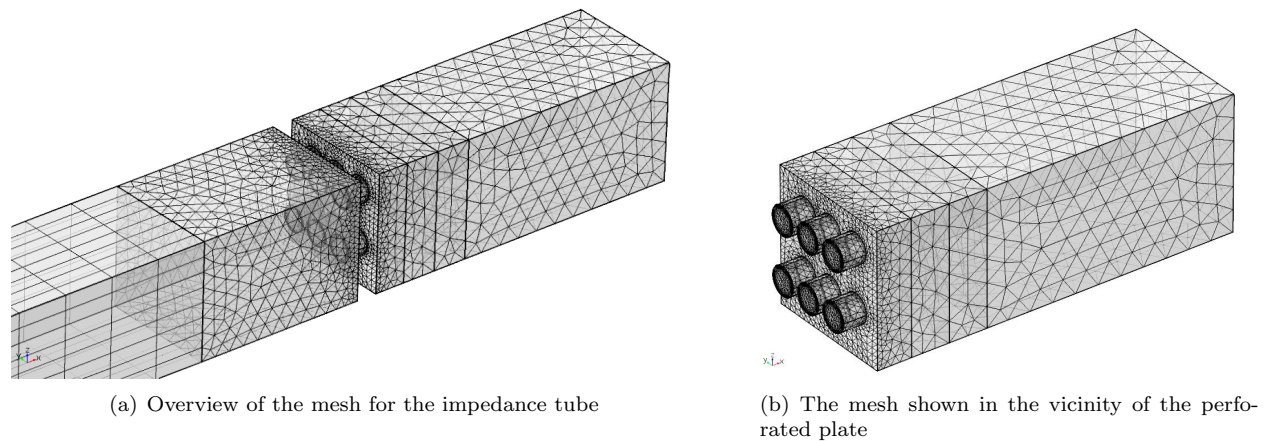


Figure 4. Overview of the mesh and the mesh in the vicinity of the perforated plate.

The mesh used in simulations is an unstructured mesh with around 700 000 elements. An overview of the mesh and the mesh in the vicinity of the perforated plate is shown in Fig. 4. A hybrid mesh mixed by tetrahedrons in the cavity, a swept mesh in the straight duct and tetrahedrons with the boundary layer mesh in the vicinity of the perforated plate is applied. With a grid element size 3mm in the main duct, there are 7 elements per wavelength for the highest frequency. All the simulations were carried out in COMSOL 5.1, which is a commercial finite element method (FEM) solver. The quadratic shape function is used in the simulations. When generating the mesh, a meshing technique for boundary layer adjustment is used, therefore the thickness of the boundary layer is adjusted depending on different frequencies. By using this technique, mesh which is able to resolve the acoustic boundary layer is produced.

IV. Validation of the continuity of the coupling conditions

In this section, the continuity of the coupling conditions between LNSE and Helmholtz equation, that is the Eqs. (14)(15)(16) is evaluated numerically. A rectangular duct with constant cross section is used as a test case. The numerical configuration of the test case is illustrated in the Fig. 5.

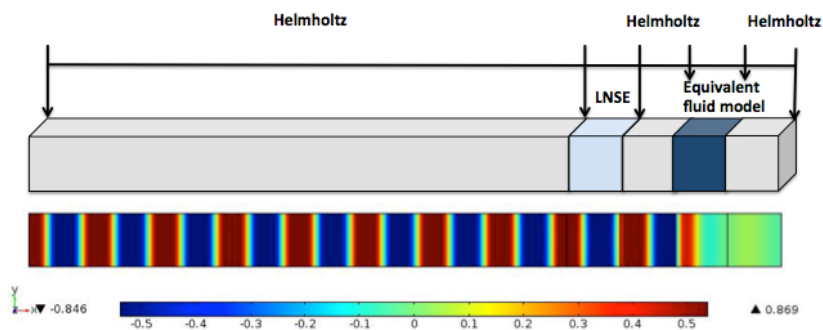


Figure 5. Schematic of the test case for the examination of the coupling conditions.

A plane wave applied at the upstream boundary, wave is first propagating through the LNSE region, then the Helmholtz region, as well as the equivalent fluid region and the Helmholtz region again.

The numerical results of the acoustic pressure contour is plotted in Fig. 5 to show the continuity of the pressure. The the pressure and the gradient of the pressure are given in Fig. 6 to show the continuity more specifically. The pink line shows the quantity solved by the Helmholtz equation (or Helmholtz type equation, since the equivalent fluid model is the Helmholtz equation with an alerted wave number) and the blue line indicates the quantity from the LNSE. It can be observed that in Fig. 6 (a) the acoustic pressure obtained by the Helmholtz equation and the LNSE is continuous without any gaps. In Fig. 6 (b), the gradient of the

acoustic pressure illustrates the continuity of the acoustics pressure as well, since any discontinuity of the acoustic pressure will reflect a jump at the discontinuous point in the gradient of the acoustic pressure.

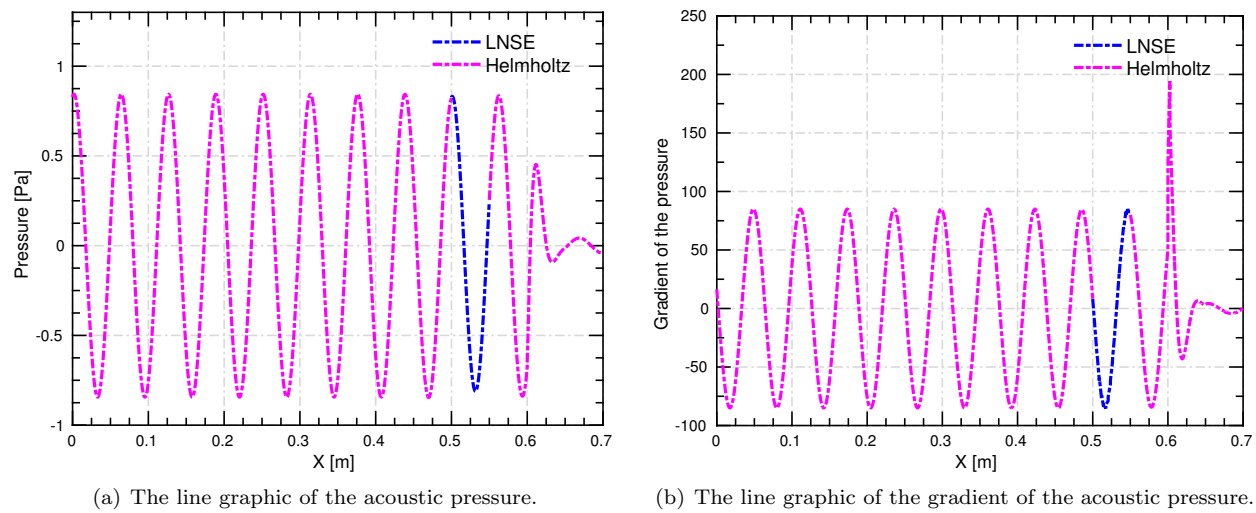


Figure 6. The line graphics of the pressure and the gradient of the pressure along the duct are presented at frequency $f = 5500Hz$.

V. Numerical Results

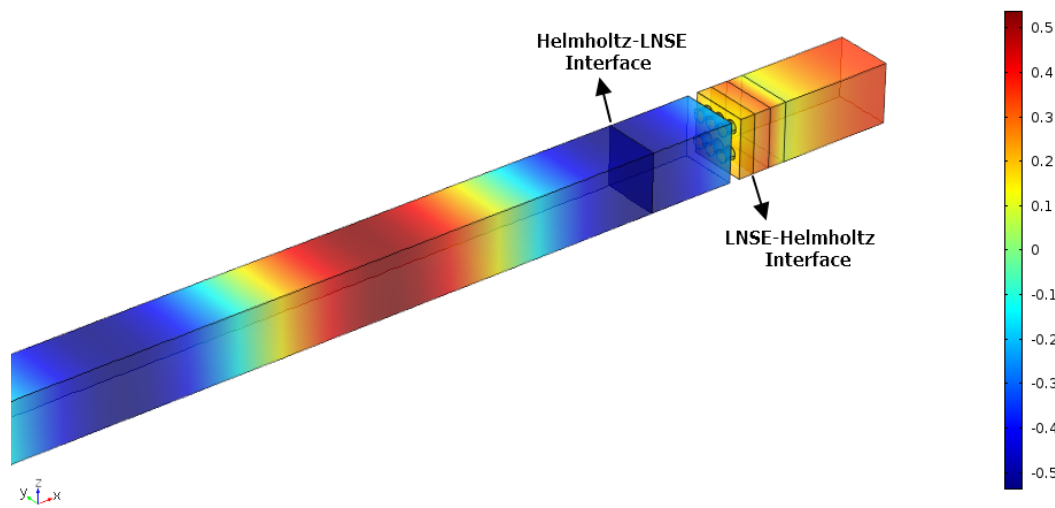


Figure 7. Three-dimensional acoustic pressure contour plot

Fig. 7 shows the three-dimensional acoustic pressure contour in the impedance tube together with the interfaces between the LNSE and the Helmholtz equation.

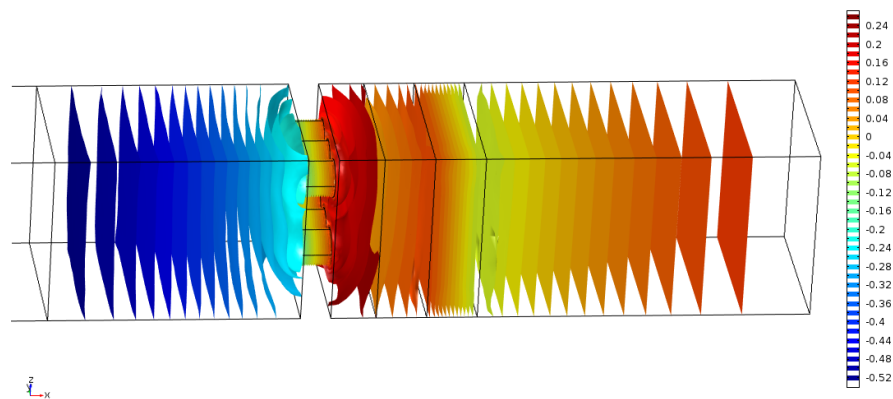
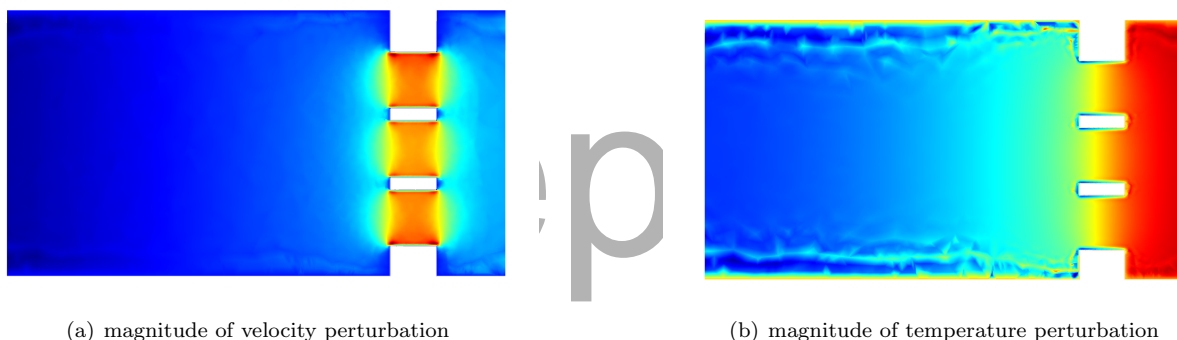


Figure 8. The isosurface of the acoustic pressure at frequency $f = 5500\text{Hz}$.

In Fig. 8, the isosurface of the acoustic pressure is plotted. It can be seen that away from the liner, the plane wave is propagating in the duct. When the wave is approaching to the hybrid liner, the isosurface are curved due to the dissipation in the acoustic boundary layer of the perforated plate. After the wave has passed through the perforated plate, it goes through the porous metallic foam region resulting in a big drop of the acoustic pressure.



(a) magnitude of velocity perturbation

(b) magnitude of temperature perturbation

Figure 9. The contour plots for magnitude of velocity perturbation and the temperature perturbation in the vicinity of the perforated plate at frequency $f = 5500\text{Hz}$.

In Fig. 9, the contour plots for the magnitude of velocity perturbation and the temperature perturbation in the vicinity of the perforated plate are presented. The air in the necks is contracting and de-contracting, meanwhile, the air in the back cavity is decompressing and compressing. The viscosity leads to an added-mass effect for the air in the necks as well as the attenuation of the sound. Further, Fig. 9 shows the temperature perturbation resolved by the linearized Navier-Stokes equations.

The plot of sound intensity indicates the acoustic energy flow as shown in Fig. 10. In the main duct where the Helmholtz equation is solved, the acoustic energy remains constant since there is no damping included in the simulations. However, when the wave is propagating in the LNSE numerical region, some acoustic energy is dissipated, leading to the change of the sound intensity. Later, the wave is propagating through the perforated plate with a much smaller cross section area. Therefore the sound intensity is higher in the small holes. In the porous region, essential damping causes the reduction of the sound intensity. In the Helmholtz cavity, the sound intensity takes the form of a vortex, since the acoustic energy is trapped in the cavity. As a result, the principle of the Helmholtz cavity is clearly visualized.

A. Comparison with and without metallic foam

In Fig. 11, the numerical results and the experimental results are presented for the hybrid liner with and without the porous metallic foam. The measurements are performed at KTH MWL by Ramio Kabral et

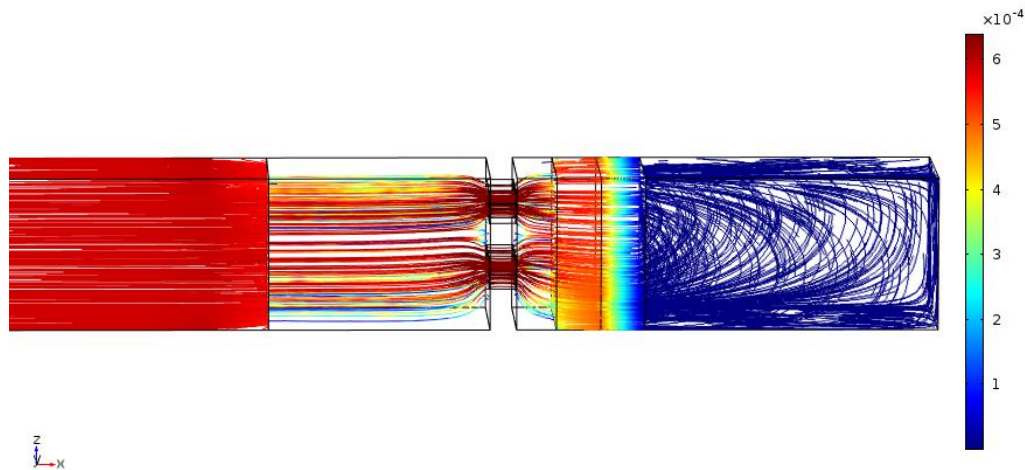


Figure 10. The acoustic flow colored by the sound intensity at frequency $f = 5500\text{Hz}$.

al.¹ A good agreement can be found between the numerical results and the experimental results, which shows that the unified approach is reliable for the hybrid liner simulations. Further, both the numerical and experimental results in Fig. 11 (a) show that with the metallic foam in the hybrid liner, the acoustic performance is enhanced almost 20%. However, the porous metallic foam only influence the phase of the reflection coefficient at frequencies lower than 3300Hz , while it doesn't influence the acoustic performance too much at the higher frequencies.

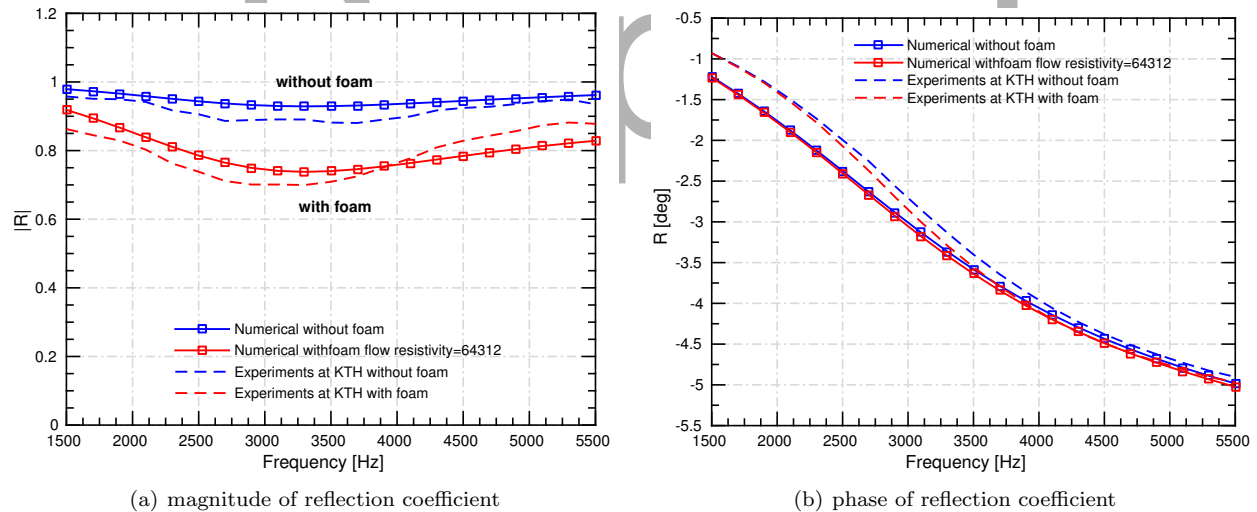


Figure 11. The magnitude (left) and phase (right) of the reflection coefficient as a function of frequency for the hybrid liner with and without the metallic foam. The thickness of the perforated plate is $t_p = 1.2\text{ mm}$. The metallic is placed close to the perforated plate, the thickness of the porous material is $t_f = 1\text{ mm}$, and the flow resistivity is $[\sigma] = 64312\text{ Nm}^{-4}\text{ s}$. Both numerical and experimental results are included in the plot.

The flow resistivity is a crucial value which determines acoustic damping in the porous metallic foam. The flow resistivity applied in the simulations in Fig. 11 is obtained from measurements. Uncertainties in the measured flow resistivity can be one reason for the slight discrepancy between the numerical and experimental results. Further, the porous metallic foam within the hybrid liner is very thin, around 1 mm and was compressed a little bit into the cavity in the experimental sample of the liner. The deformation of the metallic foam is not modelled in the numerical simulations. This may be another reason for the discrepancies. The influence of the flow resistivity and the position of the porous material are therefore

investigated below.

B. Comparison between unified approach and the Helmholtz Equation

The numerical results obtained by the unified approach with LNSE equation are compared with the numerical results obtained from only the Helmholtz equation to show the influence of the acoustic dissipation in the acoustic boundary layer. In Fig. 12, the reflection coefficient and the resistance for the two methods are shown as the functions of frequency. The numerical results indicate that with the consideration of acoustic dissipation, a 5% change for the magnitude of the reflection coefficient and for the resistance is found. The comparison of the numerical results between the unified approach and the Helmholtz equation shows that it's necessary to take the acoustic dissipation into account in the further simulations. However, the acoustic dissipation doesn't make too much influence on the phase or reactance.

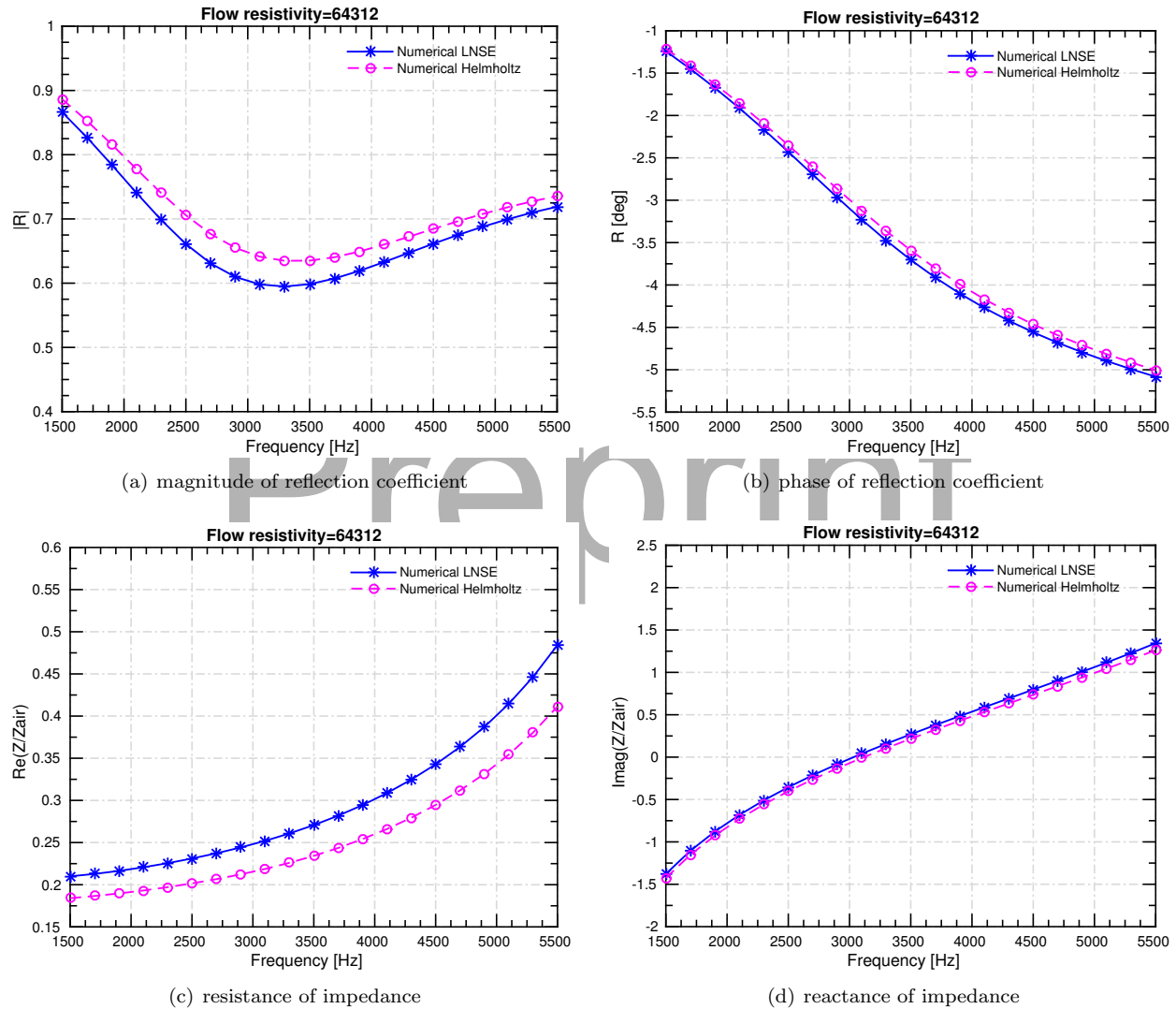


Figure 12. The magnitude (upper left), phase (upper right) of the reflection coefficient, the resistance (lower left) and the reactance (lower right) as a function of frequency for the hybrid liner with the metallic foam. The thickness of the perforated plate is $t_p = 1.2 \text{ mm}$, the thickness of the porous material is $t_f = 1 \text{ mm}$, and the flow resistivity is $[\sigma] = 64312 \text{ Nm}^{-4}\text{s}$. Numerical results from the Unified approach and the numerical results from only the Helmholtz equation are included in the plot.

C. Comparison with different flow resistivity

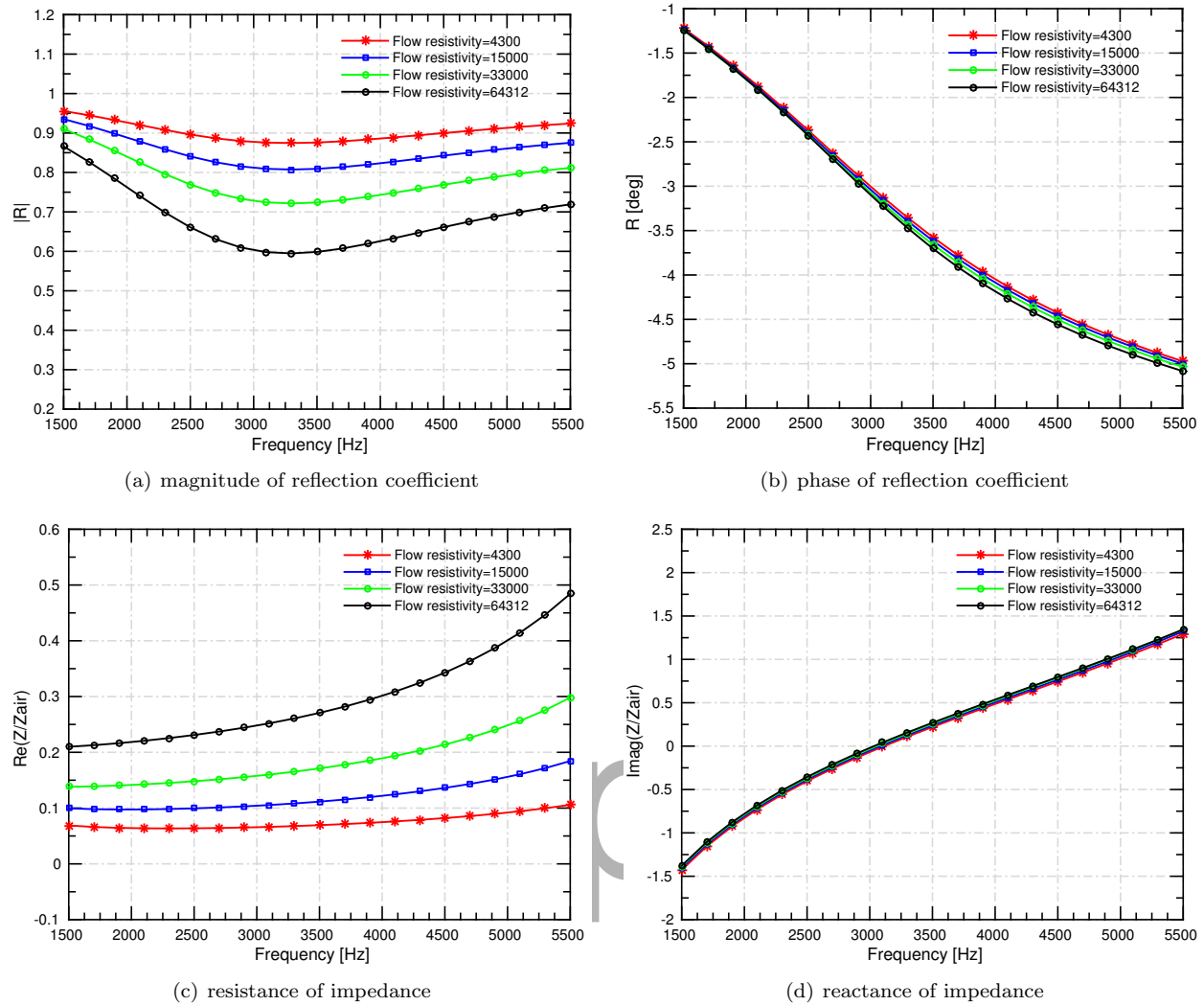


Figure 13. The magnitude (upper left), phase (upper right) of the reflection coefficient, resistance (lower left) and reactance (lower right) as a function of frequency for the hybrid liner with the metallic foam. The thickness of the perforated plate is $t_p = 1.2$ mm, the thickness of the porous material is $t_f = 1$ mm, and the flow resistivity is varying as the figures show, such as $[\sigma] = 4300$ $Nm^{-4}s$, $[\sigma] = 15000$ $Nm^{-4}s$, $[\sigma] = 33000$ $Nm^{-4}s$ and $[\sigma] = 64312$ $Nm^{-4}s$. Numerical results for the acoustic hybrid liner with different flow resistivity are included in the plot.

The numerical results presented in Fig. 13. show the sensitivity of flow resistivity to the acoustic performance of the hybrid liner. Each flow resistivity, it stands for different material, e.g. $[\sigma] = 4300$ $Nm^{-4}s$ refers to the glass fibre (G1), $[\sigma] = 15000$ $Nm^{-4}s$ refers to the mineral fibre (M2), $[\sigma] = 33000$ $Nm^{-4}s$ stands for the mineral fibre (M2-40 mm) and the $[\sigma] = 64312$ $Nm^{-4}s$ stands for the material of the experimental sample, a high density metallic foam. When the flow resistivity is increasing from the 4300 to 64312, the magnitude of the reflection coefficient is reduced maximum around 30% at frequency ranges between 3000 Hz to 4000 Hz. With the increasing flow resistivity for porous material, the hybrid liner always gives a better acoustic performance. The liner with different design parameters, such as thickness of the perforated plate and different porosity etc, has been simulated in the previous papers.⁹

D. Comparison for the location of the porous metallic foam

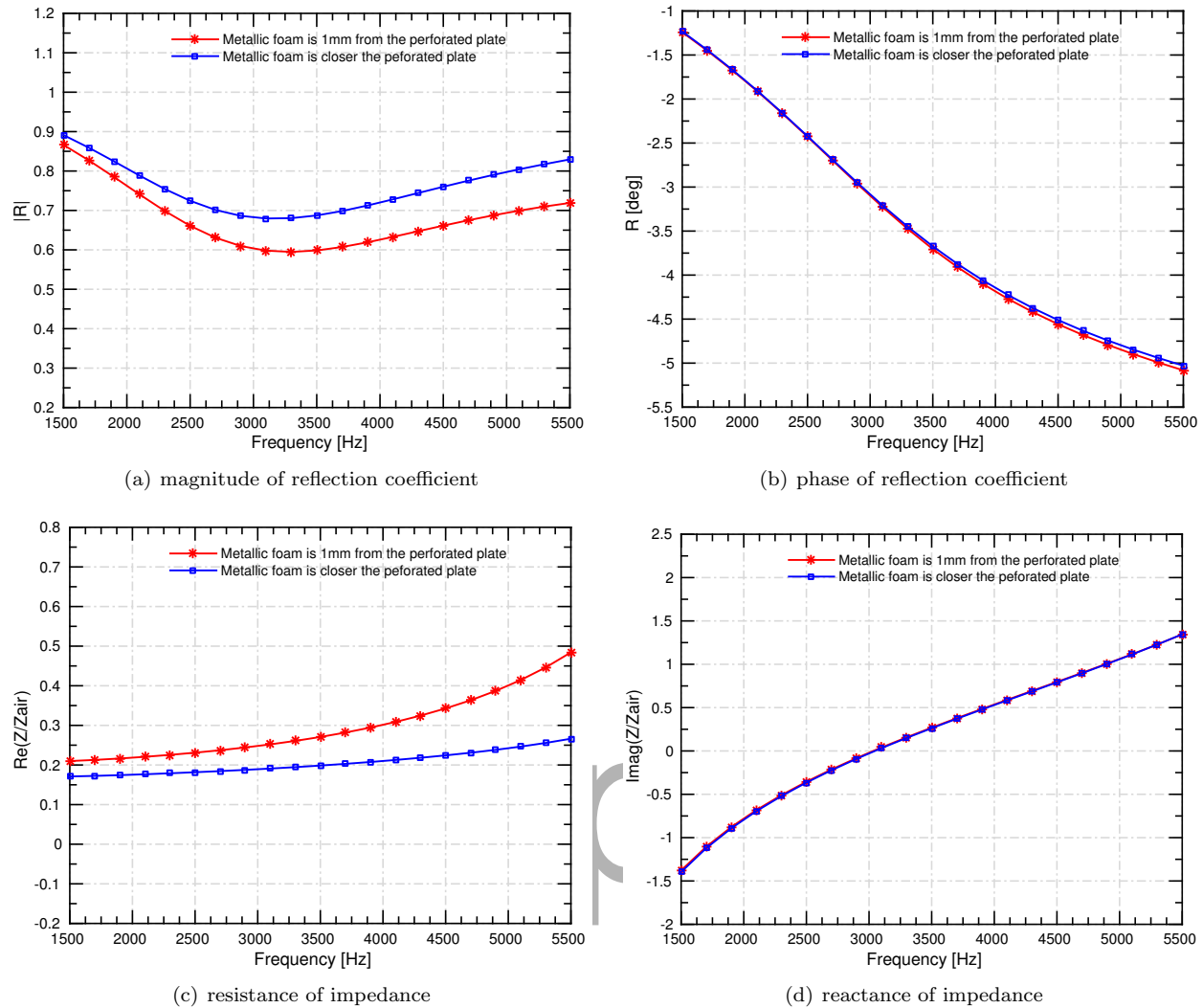


Figure 14. The magnitude (upper left), phase (upper right) of the reflection coefficient, resistance (lower left) and reactance (lower right) as a function of frequency for the hybrid liner with the metallic foam. The thickness of the perforated plate is $t_p = 1.2 \text{ mm}$, the thickness of the porous material is $t_f = 1 \text{ mm}$, and the flow resistivity is $[\sigma] = 64312 \text{ Nm}^{-4}\text{s}$. In one numerical case, the metallic foam is placed 1mm from the perforated plate, in another numerical case, the metallic foam is placed next to the perforated plate.

Fig. 14 shows the reflection coefficient and the impedance of the hybrid liner when the metallic foam is placed at different locations. In one case the metallic foam is placed 1mm from the perforated plate, while in another case the metallic foam is placed next to the perforated plate. In Fig. 14 (a) and (c), the acoustic performance changes around 10% between 3000Hz and 5500Hz for these two different numerical cases. The numerical results show that when the porous metallic foam is placed a little bit away from the perforated plate, the absorption will increase, on the contrary, when the metallic foam is placed next to the perforated plate resulting in less absorption. This may be due to some contraction and expansion at the end of the small holes in the perforated plate, and hence the installation of the metallic foam close to the perforated plate will have a large influence.

Conclusion

In this paper, we present the numerical methodology - the unified approach in frequency domain to predict the acoustic performance of a hybrid liner, which is made of a perforated plate, a metallic foam and

a rectangular back cavity. The coupling conditions to connect the LNSE and the Helmholtz equation are validated.

Acoustic performances for the hybrid liner with and without the porous metallic foam, with different flow resistivity and with the porous foam at different locations are obtained from the simulations. All the numerical results are compared with the measurements performed at KTH MWL. It can be observed that the numerical results are in good agreement with the results from the measurements. Generally, the inclusion of the porous metallic foam is an effective way to enhance the absorption of the acoustic liners. In particular, the placement of the metallic foam has a rather large influence on the performance of the hybrid liner.

Acknowledgments

The presented work is part of the Marie Curie Initial Training Network Thermo-acoustic and aero-acoustic nonlinearities in green combustors with orifice structures (TANGO). We gratefully acknowledge the financial support from the European Commission under call FP7-PEOPLE-ITN-2012.

References

- ¹Raimo Kabral, Hans Bodén Lin Zhou, and Tamer Elnady. Determination of liner impedance under high temperature and grazing flow conditions. *18th AIAA/CEAS Aeroacoustics Conference*, 2014.
- ²A. Kierkegaard, S. Boij, and G. Efraimsson. A frequency domain linearized navier-stokes equations approach to acoustic propagation in flow ducts with sharp edges. *The Journal of the Acoustical Society of America*, 127(2):710–719, 2010.
- ³Axel Kierkegaard, Gunilla Efraimsson, and Anurag Agarwal. Simulations of a liner cell using a frequency-domain linearized navier-stokes methodology. In *19th AIAA/CEAS Aeroacoustics Conference*, 2013.
- ⁴A. Kierkegaard, S. Allam, G. Efraimsson, and M. Åbom. Simulations of whistling and the whistling potentiality of an in-duct orifice with linear aeroacoustics. *Journal of Sound and Vibration*, 331(5):1084–1096, 2012.
- ⁵G. K. Batchelor. *An Introduction to Fluid Dynamics*. Cambridge mathematical library. Cambridge University Press, 2000.
- ⁶Chenyang Weng. Theoretical and numerical studies of sound propagation in low-mach-number duct flows. 2015.
- ⁷A. D. Pierce. *Acoustics: An Introduction to Its Physical Principles and Applications*. the Acoustical Society of America, 1991.
- ⁸Jean Allard and Noureddine Atalla. *Propagation of sound in porous media: modelling sound absorbing materials 2e*. John Wiley & Sons, 2009.
- ⁹Wei Na, Susann Boij, and Gunilla Efraimsson. Simulations of acoustic wave propagation in an impedance tube using a frequency-domain linearized navier-stokes methodology. *20th AIAA/CEAS Aeroacoustics Conference*, Jun 2014.

Preprint